Available online at www.sciencedirect.com
ScienceDirect
Journal of Power Sources 175 (2008) 558–563
JOURNAL OF POWER SOURCES
www.elsevier.com/locate/jpowsour

Short communication

Nano-sized $SnSbCu_x$ alloy anodes prepared by co-precipitation for Li-ion batteries

Fei Wang *, Mingshu Zhao, Xiaoping Song

Department of Materials Physics, School of Science, Xi'an Jiaotong University, Xi'an 710049, PR China

Received 18 March 2007; received in revised form 17 August 2007; accepted 27 September 2007
Available online 2 October 2007

Abstract

Nano-sized $SnSbCu_x$ alloy anode materials are prepared by reductive co-precipitation method combining with the aging treatment in water bath at 80 °C. The microstructure, morphology and electrochemical properties of synthesized $SnSbCu_x$ alloy powders are evaluated by X-ray diffraction (XRD), field-emission scanning electron microscopy (FE-SEM) and galvanostatical cycling tests. The results indicate that the average particle size is reduced and the Cu_6Sn_5, Cu_2Sb phases appear successively along with the increase of Cu content in the $SnSbCu_x$ alloy. The reduction of average particle size, the existence of inactive element Cu and the complex multi-step reaction mechanism in $SnSbCu_x$ alloy anodes are propitious to improve the structure stability and thus improve the cycling performance. When cycled at a constant current density of 0.1 mA cm^{-2} between 0.02 and 1.50 V, the coulomb efficiency of first cycle exceeds 74% and the reversible capacity of 20th cycle attains to 490 mAh g^{-1} in $SnSbCu_{0.5}$ alloy anode.

Keywords: Lithium-ion battery; Anode; Nano-sized; $SnSbCu_x$ alloy; Cycling performance

1. Introduction

Rechargeable lithium-ion batteries are widely used in various electronic devices, because they are easily formed into different shapes and show no memory effect and low self-discharge rate, etc. With the increasing demand of higher performance, the common commercial Li-ion batteries with graphite anode and $LiCoO_2$ cathode cannot satisfy the demanding, which stimulates researchers to explore novel electrode materials to substitute the traditional materials.

There are many lithium storage metals and alloys such as Sn, Sb, Al, Si, Cu–Sn, Sn–Sb, Ag–Sn, Si–Sn, etc., which can offer much higher energy density and specific capacity than that of the traditional carbon materials. So they are regarded as possible new anode material for lithium-ion batteries. For these metals/alloys anode materials, SnSb-based alloy anodes have received much attention and intensive investigation for its numerous merits [1–14]. The theoretical Li storage capacity of SnSb alloy anode is very high and approaches that of the pure metals, since both components of SnSb alloy are active for Li storage. The Li-insertion potential of Sn (below 0.5 V vs. Li/Li^+) and Sb (around 0.8 V vs. Li/Li^+) is different, when one component reacts with Li, the other component can "buffer" the volume change of the reacting one. In addition, SnSb alloy electrode has reversible phase transition during Li-insertion/extraction process, in which the strong structural relationship exhibits between the parent binary intermetallic electrode and its lithiated product [15,16]. Furthermore, Sn and Sb are cheap and environmental friendly. However, the materials mentioned above (including SnSb alloy) undergo severe volume expansion and contraction during the lithiation and de-lithiation processes. This greatly limits the mechanical stability and cycle life of the electrode materials and thus limits their actual application.

To overcome this problem, consistent efforts have been devoted to improve the cycling performance of metals/alloys anode materials and several strategies have been brought out. Among them, reducing particle size of alloy anode materials into nanometer scale is considered as an efficient way. The reducing of particle size can reduce the absolute volume variation and ion diffusion length during the lithiation and delithiation processes. However, reducing particle size

* Corresponding author. Tel.: +86 29 82675055; fax: +86 29 82667872.
E-mail address: feiwang@mail.xjtu.edu.cn (F. Wang).

0378-7753/$ – see front matter © 2007 Elsevier B.V. All rights reserved.
doi:10.1016/j.jpowsour.2007.09.087

will result in a large initial irreversible capacity and other new problems [1,2]. So, we attempt to combine the reducing of particle size with other strategy to improve the cycling performance of alloy anodes.

In this work, we choose SnSb alloy as the matrix anode material because of its attractive merits mentioned above and add a tertiary element Cu to it. The existence of Cu can reduce the average particle size of the alloy powders and Cu also acts as an inactive matrix during whole electrochemical reaction process. The reductive co-precipitation is a simple method to obtain nano-sized alloy anode materials. In order to improve the morphology and electrochemical property of the alloy anode materials prepared by reductive co-precipitation, we treated with the freshly precipitated alloy particles by aging in constant temperature water bath at 80 °C. Our work shows that the aging treatment is a simple and efficient method to obtain comparative uniform phase components, integrated particles and good electrochemical performance [17].

2. Experimental

Nano-sized alloy powders were synthesized by reductive co-precipitation method in our studies. To produce the $SnSbCu_x$ alloy powders, 0.01 mol $SnCl_2{\bullet}2H_2O$, 0.01 mol $SbCl_3$, x mol ($x = 0$, 0.003, 0.005, 0.01) $CuCl_2{\bullet}2H_2O$ and y mol ($y = 0.035$, 0.038, 0.04, 0.045) $C_6H_5Na_3O_7{\bullet}2H_2O$ were mixed together and dissolved in 100 ml distilled water to form a 0.1 M solution of Sn^{2+}. The 0.2 M alkaline $NaBH_4$ aqueous solution (pH >12) was added drop wise to the above mixed aqueous solution under strong magnetic stirring at room temperature. The superfluous $NaBH_4$ solution was used to ensure a complete reduction of the metal ions. Furthermore, the SnSb alloy with small particle size (marked SnSb′) were synthesized at the same conditions except the reaction mode. To synthesize SnSb′ alloy, the mixed aqueous solution was added drop wise to alkaline $NaBH_4$ aqueous solution. After co-precipitation, all alloy powders in the aqueous solution were aged in the water bath with a constant temperature of 80 °C for 5 h. Then, the solution was filtered and the product was washed thoroughly using distilled water and acetone. The black product was dried at 105 °C for 10 h under vacuum.

The crystal structure of alloy anode materials was detected by Shimadzu-7000 type X-ray diffraction with Cu Kα radiation ($\lambda = 1.5406$). The morphology and particle size of the alloy powders were observed by JSM-6700 type field-emission scanning electron microscopy.

Electrochemical experiments were carried out in two-electrode Swagelok cells which was composed of a metallic lithium foil as counter electrode, 1 M LiPF6 in ethylene carbonate (EC)–diethyl carbonate (DEC) (1:1, v/v) as electrolyte, Celegard 2400 as separator and nano-sized alloy as the working electrode. The working electrodes were prepared by pasting slurry onto a copper foil substrate. The slurry consisted of 80 wt% alloy powder, 10 wt% acetylene black and 10 wt% polyvinylidene fluoride (PVDF) dissolved in NMP. Then the electrodes were dried in vacuum oven at 110 °C for 12 h prior to use. Testing cells were assembled in an argon-filled glove box and were cycled on the Arbin BT2000 battery tester at a constant current density of 0.1 mA cm^{-2} between 0.02 and 1.50 V.

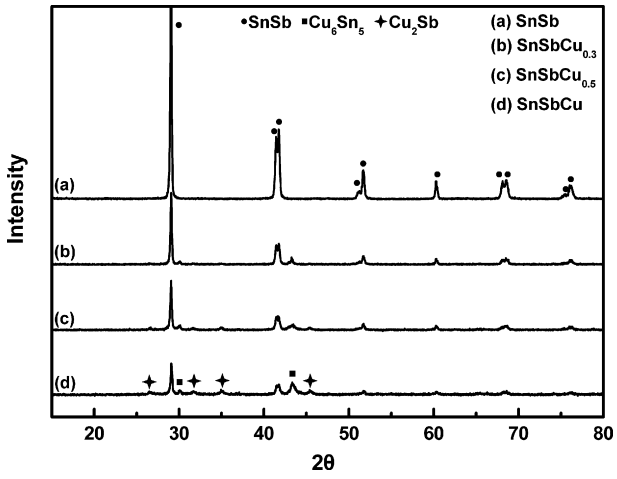

Fig. 1. XRD patterns of different $SnSbCu_x$ alloy powders prepared by reductive co-precipitation method.

3. Results and discussion

The X-ray diffraction patterns of $SnSbCu_x$ alloy powders are shown in Fig. 1. The pure SnSb alloy shows a single phase as depicted in the diffraction pattern of Fig. 1(a). However, the second phase of Cu_6Sn_5 begins to appear when Cu exists in the $SnSbCu_{0.3}$ alloy, as shown in Fig. 1(b). With the further increase of Cu content, the third phase of Cu_2Sb begins to appear. As shown in Fig. 1(c) and (d), the SnSb, Cu_6Sn_5 and Cu_2Sb phases coexist in the $SnSbCu_x$ alloy when x (the atom ratio of Cu to Sn/Sb) is larger than 0.5. From Fig. 1 we can also see that the intensity of diffraction peak is reduced markedly along with the increase of Cu content. Furthermore, from the intensity evolution among the diffraction peaks, we can conclude that the contents of Cu_6Sn_5 and Cu_2Sb phases increase and that of SnSb phase decreases continuously along with the increase of Cu content in the $SnSbCu_x$ alloy.

Fig. 2 shows the FE-SEM images of $SnSbCu_x$ alloy powders prepared by reductive co-precipitation method. From Fig. 2(a) we can see that the particle size of SnSb alloy powders is large and relatively uniform. When the content of Cu is increased in the $SnSbCu_x$ alloy, the average particle size of alloy powders is reduced and the particle size becomes nonuniform, as shown in Fig. 2(b) and (c). From the peak position and the half-height width of the X-ray diffraction peak, the mean crystallite size can be calculated by Scherrer equation. The results are shown in Table 1. From it we can see clearly that the mean crystallite size of SnSb phase is large and that of Cu_6Sn_5 and Cu_2Sb phases is small. So, the large particles in Fig. 2(b) and (c) should be SnSb alloy and the small particles are composed of Cu_6Sn_5, Cu_2Sb and part of SnSb alloys. Along with the increase of Cu content, the content of Cu_6Sn_5 and Cu_2Sb phases improves and the growing of SnSb particles through atom diffusing is restrained in some degree, so the average particle size of $SnSbCu_x$ alloy powders is reduced markedly. These are consistent with the intensity evolution of diffraction peak. Furthermore, along with the reducing

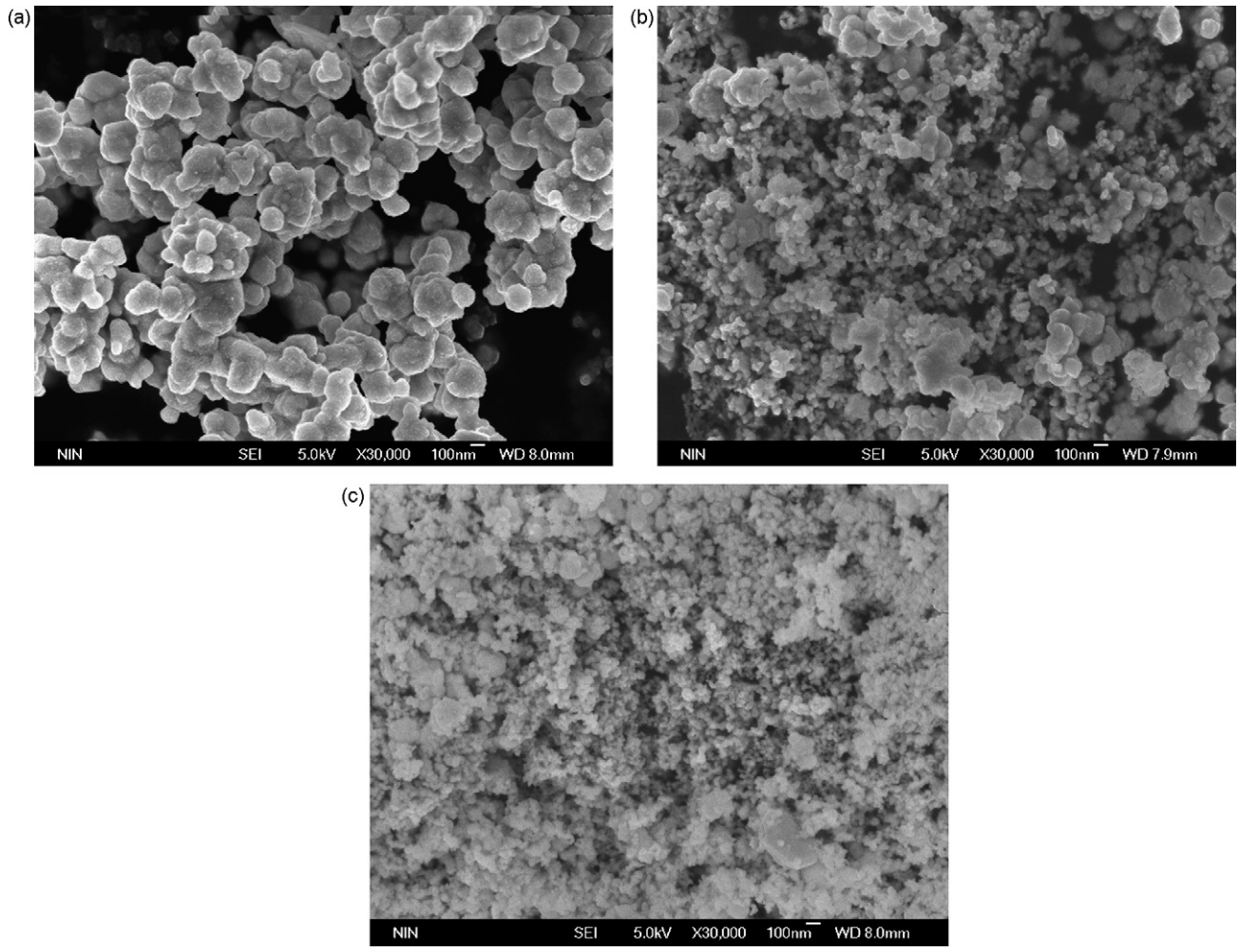

Fig. 2. FE-SEM images of different $SnSbCu_x$ alloy powders prepared by reductive co-precipitation method: (a) SnSb, (b) $SnSbCu_{0.5}$, (c) SnSbCu.

of particle size, the alloy powders become easy to be oxidized in the air. It is difficult to get clear images of SnSbCu alloy powders because of the conductivity reducing caused by surface oxides.

The voltage versus specific capacity curves measured in the first cycle of different $SnSbCu_x$ alloy electrodes are shown in Fig. 3. In the discharge process, all voltage curves exhibit a rapid voltage drop above 0.75 V, which attribute to some irreversible reactions such as the decomposition of electrolyte, the reduction of oxide impurity and the formation of solid electrolyte interphase (SEI) film. These irreversible reactions mainly lie on the specific surface area and surface oxide of the alloy powders. The particle size of $SnSbCu_x$ alloy powders is reduced obviously along with the increase of Cu content, i.e., the specific surface area and surface oxide are increased. So the more Cu

Table 1
The phase composition and mean crystallite size of $SnSbCu_x$ alloy powder

Sample	Phase composition	Mean crystallite size (nm)
SnSb	SnSb	64.7
$SbSbCu_{0.3}$	SnSb	57.2
	Cu_6Sn_5	
$SbSbCu_{0.6}$	SnSb	50.5
	Cu_6Sn_5	21.8
	Cu_2Sb	
SbSbCu	SnSb	48.3
	Cu_6Sn_5	17.0
	Cu_2Sb	17.9

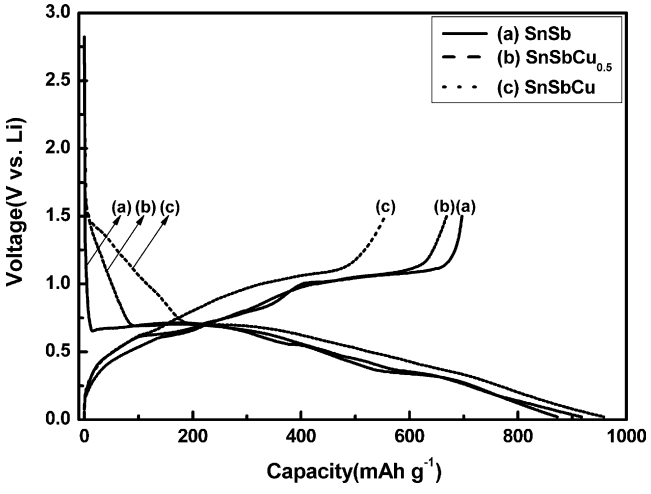

Fig. 3. Initial voltage profiles of different $SnSbCu_x$ alloy electrodes.

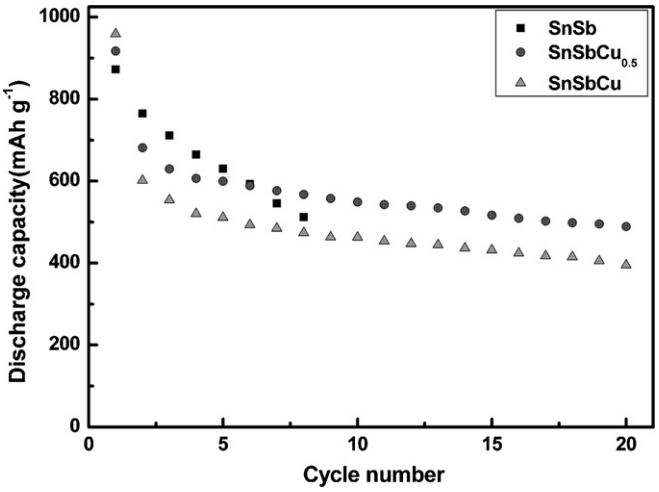

Fig. 4. Cycling performances of different $SnSbCu_x$ alloy electrodes.

exists in $SnSbCu_x$ alloy, the more irreversible capacities exist. When electrodes discharge below 0.75 V, the discharge voltage curves of different $SnSbCu_x$ alloy electrodes are similar, which corresponds to the reversible reaction of Li with Sb and Sn at different stages. During the charge process, the voltage versus specific capacity curves of different $SnSbCu_x$ alloy electrodes show similar behavior, too. The main different is that the charge capacities in the first cycle reduce gradually along with the increase of Cu content. It attributes to the more irreversible reaction illustrated above and the more irreversible trapping of insert Li-ions, which is caused by more high energy intrinsic and extrinsic defects existed in the sample with smaller particle size.

From Fig. 3 we can conclude that the reversible capacities of SnSb alloy electrode are much higher than that of ternary $SnSbCu_x$ alloy electrodes in the first cycle. However, the pure SnSb electrode cannot keep such attractive high capacities in the subsequent cycles. As depicted in Figs. 4 and 5, the capacity of SnSb electrode decreases obviously in every cycle and the coulomb efficiency of every cycle do not exceed 95%. On the contrary, the ternary $SnSbCu_x$ alloy electrodes show better cycling performance than pure SnSb electrode. For example, the capacities of $SnSbCu_{0.5}$ electrode decrease slowly and the coulomb efficiency of every cycle exceed 98% after first three cycles. It should be noted that the capacity of $SnSbCu_{0.5}$ electrode exceeds that of the SnSb electrode only after seven cycles, despite that the initial capacity of SnSb electrode far exceeds that of $SnSbCu_{0.5}$ electrode. Up to 20 cycles, the $SnSbCu_{0.5}$ electrode exhibits excellent cycling performance and delivers large reversible capacities above 490 mAh g^{-1}.

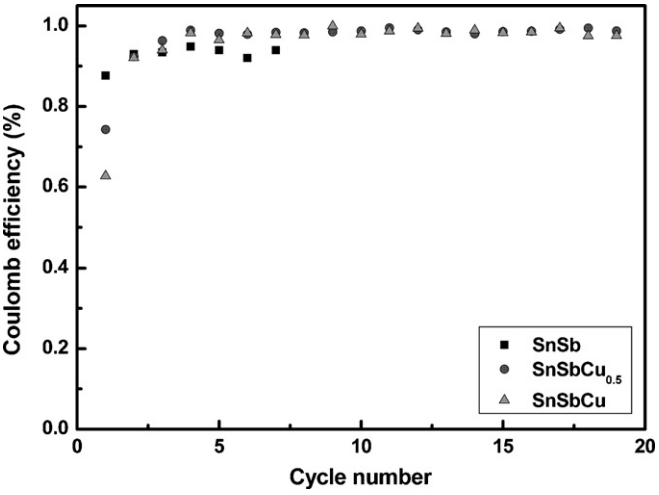

Fig. 5. Coulomb efficiency of different $SnSbCu_x$ alloy electrodes.

The difference of cycling performance between SnSb and $SnSbCu_{0.5}$ alloy electrodes is strongly related with their morphology before and after cycling. As shown in Figs. 2 and 6, the morphology change of SnSb and $SnSbCu_{0.5}$ alloy electrodes after eight cycles is clarified by FE-SEM images. From Fig. 6(a) we can see clearly that the original SnSb particles become larger and obviously tend to pulverize due to drastic volume variation during the lithiation and de-lithiation processes. However, we have not seen similar tendency in $SnSbCu_{0.5}$ alloy powders.

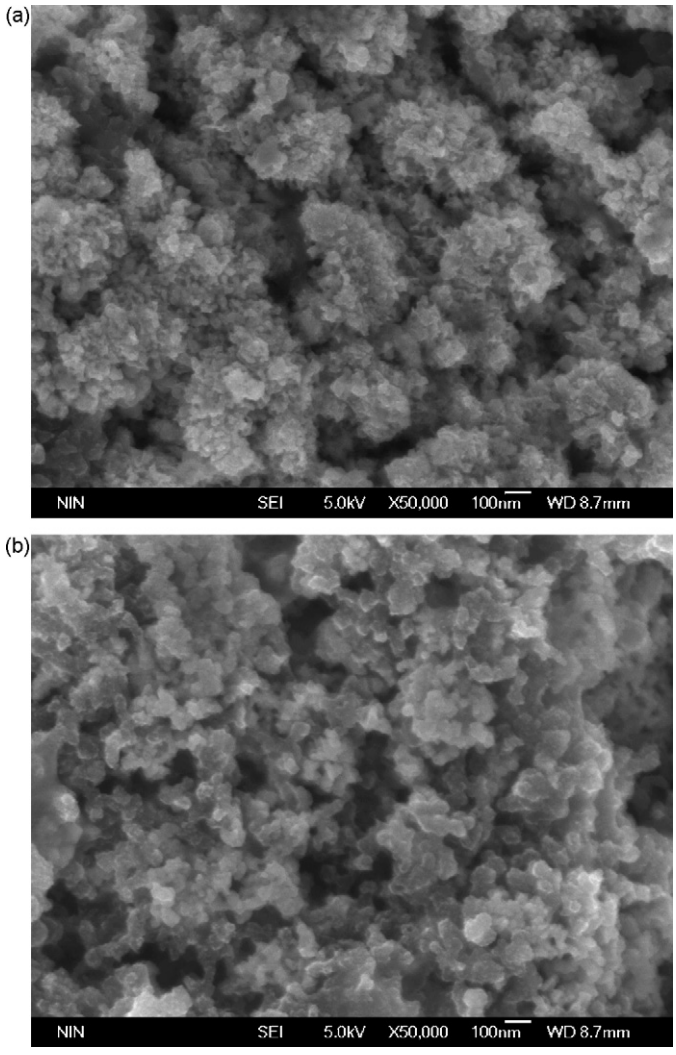

Fig. 6. FE-SEM images of different alloy electrodes after eight cycles: (a) SnSb and (b) $SnSbCu_{0.5}$.

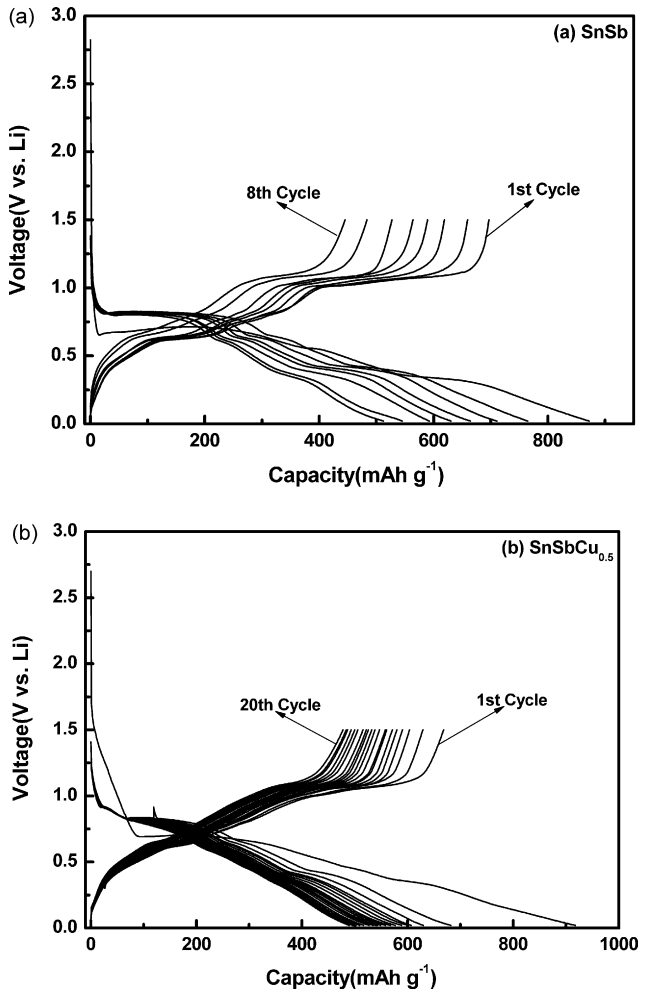

Fig. 7. Voltage profiles of different alloy electrodes: (a) SnSb and (b) $SnSbCu_{0.5}$.

The difference of these morphology changes may be caused by the following factors. At first, the reducing of particle size induced by Cu existing results in smaller absolute volume variation and shorter Li-ion diffusion length. Secondly, the existence of inactive element Cu can buffer the volume changes of active phases Sn and Sb. Thirdly, the "dense" multi-step reaction in $SnSbCu_{0.5}$ make the whole lithiation/de-lithiation reaction take place in a relatively slow change process. This was depicted in the voltage profiles of SnSb and $SnSbCu_{0.5}$ alloy electrodes, as shown in Fig. 7. The voltage profile of pure SnSb electrode has several distinct voltage plateaus, which correspond to the formation of Li_3Sb and a series of Li–Sn alloy. However, the voltage plateaus of $SnSbCu_{0.5}$ electrode are difficult to distinguish. The smooth voltage profile of $SnSbCu_{0.5}$ electrode can be attributed to the "dense" multi-step reaction. From Fig. 1(c) we can see clearly that the $SnSbCu_{0.5}$ alloy is composed of three phases: SnSb, Cu_6Sn_5 and Cu_2Sb. In lithiation/de-lithiation process, each of them has several voltage plateaus in different position. Because even the same active element has a little discriminating voltage plateaus when they exist in different phase composition, such as Li–Sn in SnSb, Cu_6Sn_5 and Li–Sb in SnSb and Cu_2Sb. When these "dense" voltage plateaus in different position integrate into one voltage curve, a relatively smooth voltage curve

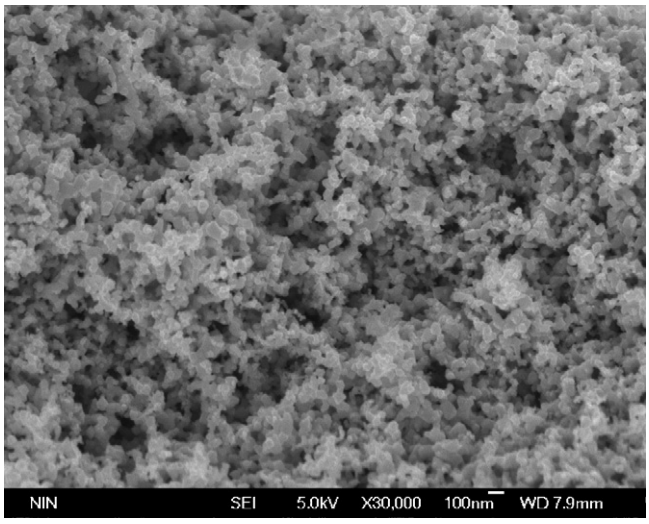

Fig. 8. FE-SEM image of SnSb′ alloy powders prepared by reductive co-precipitation method.

appears. This complex multi-step reaction in $SnSbCu_{0.5}$ electrode would reduce the absolute volume variation in every step and make the whole lithiation/de-lithiation reaction take place in a relatively slow change process. The three reasons mentioned above must be propitious to improve the stability of structure and thus improve the cycling performance.

Fig. 4 also compares the cycling performance of $SnSbCu_{0.5}$ and SnSbCu alloy electrodes. Both $SnSbCu_{0.5}$ and SnSbCu have good cycling performance. But the SnSbCu electrode has higher initial irreversible capacities and lower reversible capacities compared with that of $SnSbCu_{0.5}$ electrode. So more inactive Cu existed in $SnSbCu_x$ alloy will deteriorate the electrochemistry performance of the $SnSbCu_x$ alloy anode. In this study, $SnSbCu_{0.5}$ alloy anode has the best integrated performance.

It should be noted that the existence of Cu in $SnSbCu_{0.5}$ alloy anode improves the cycling performance markedly, and the sacrifice of reversible capacity and initial coulomb efficiency is moderate. The coulomb efficiency of first cycle exceeds 74% and the reversible capacity of 20th cycle attains to 490 mAh g^{-1}

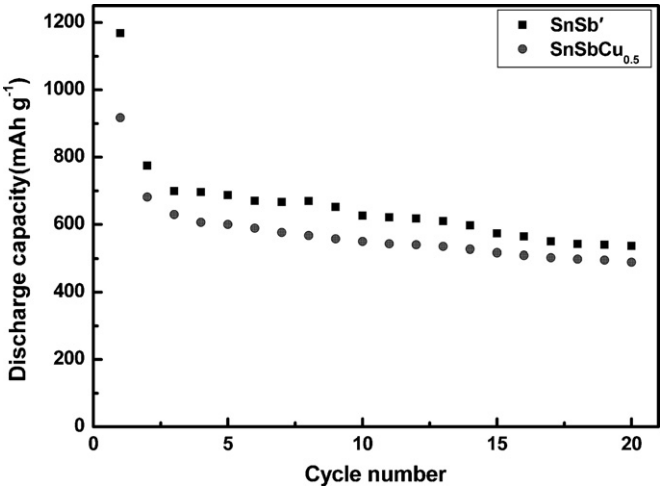

Fig. 9. Cycling performances of SnSb′ and $SnSbCu_{0.5}$ alloy electrodes.

in $SnSbCu_{0.5}$ alloy anode. As a compare, we also prepared the SnSb′ alloy with small particle size, which is the usual method to improve the cycling performance of SnSb alloy. From Fig. 8 we can see clearly that the particle size of SnSb′ alloy is far less than that of SnSb alloy. The cycling performance of SnSb′ alloy is comparable to $SnSbCu_{0.5}$ alloy, but the initial irreversible capacity of SnSb′ alloy is too high to acceptable, as shown in Fig. 9.

4. Conclusions

In this work we have investigated the $SnSbCu_x$ alloy anode materials by reductive co-precipitation method combining with the aging treatment in water bath at 80 °C. Compared with different $SnSbCu_x$ alloy anode materials, the $SnSbCu_{0.5}$ alloy anode have the best integrated performance. It is proved that the existence of Cu in $SnSbCu_{0.5}$ alloy anode can improve the cycling performance markedly, and the sacrifice of initial coulomb efficiency and reversible capacity is moderate. When cycled at a constant current density of 0.1 mA cm^{-2} between 0.02 and 1.50 V, the coulomb efficiency of first cycle exceeds 74% and the reversible capacity of 20th cycle attains to 490 mAh g^{-1} in the $SnSbCu_{0.5}$ alloy anode.

Acknowledgements

We greatly appreciate the help of Prof. Y.C. Zhai (School of Materials and Metallurgy, Northeastern University) for measurement. This work was supported by Introduction of Talents Fund of Xi'an Jiaotong University (Grant No. 090071181).

References

[1] H. Li, L.H. Shi, W. Lu, X.J. Huang, L.Q. Chen, J. Electrochem. Soc. 148 (2001) A915–A922.
[2] H. Li, L.H. Shi, Q. Wang, L.Q. Chen, X.J. Huang, Solid State Ionics 148 (2002) 247–258.
[3] A. Trifonova, M. Wachtler, M.R. Wagner, H. Schroettner, Ch. Mitterbauer, F. Hofer, K.C. Möller, M. Winter, J.O. Besenhard, Solid State Ionics 168 (2004) 51–59.
[4] H. Mukaibo, T. Osaka, P. Reale, S. Panero, B. Scrosati, M. Wachtler, J. Power Sources 132 (2004) 225–228.
[5] J. Yang, M. Wachtler, M. Winter, J.O. Besenhard, Electrochem. Solid State Lett. 2 (1999) 161–163.
[6] H. Li, G.Y. Zhu, X.J. Huang, L.Q. Chen, J. Mater. Chem. 10 (2000) 693–696.
[7] J. Yang, Y. Takeda, N. Imanishi, J.Y. Xie, O. Yamamoto, Solid State Ionics 133 (2000) 189–194.
[8] I. Rom, M. Wachtler, I. Papst, M. Schmied, J.O. Besenhard, F. Hofer, M. Winter, Solid State Ionics 143 (2001) 329–336.
[9] M. Wachtler, J.O. Besenhard, M. Winter, J. Power Sources 94 (2001) 189–193.
[10] M. Wachtler, M. Winter, J.O. Besenhard, J. Power Sources 105 (2002) 151–160.
[11] S.A. Needham, G.X. Wang, H.K. Liu, J. Alloy Compd. 400 (2005) 234–238.
[12] F.J.F. Madrigal, P. Lavela, C.P. Vicente, J.L. Tirado, Chem. Mater. 14 (2002) 2962–2968.
[13] H.L. Zhao, D.H.L. Ng, Z.Q. Lu, N.G. Ma, J. Alloy Compd. 395 (2005) 192–200.
[14] L. Balan, R. Schneider, D. Billaud, J. Lambert, J. Ghanbaja, Mater. Lett. 59 (2005) 2898–2902.
[15] M.M. Thacheray, J.T. Vaughey, C.S. Johnson, A.J. Kropf, R. Benedek, L.M.L. Fransson, K. Edstrom, J. Power Sources 113 (2003) 124–130.
[16] R. Benedek, M.M. Thacheray, J. Power Sources 110 (2002) 406–411.
[17] F. Wang, M.S. Zhao, X.P. Song, J. Alloy Compd. 439 (2007) 249–253.